Generator coordinate calculations for breathing-mode giant monopole resonance in the relativistic mean-field theory

M.V. Stoitsov,[1,*] P. Ring,[1] and M.M. Sharma[2]
[1] *Physik Department, Technische Universität München, D-85748 Garching, Germany*
[2] *Max Planck Institut für Astrophysik, Karl-Schwarzschild-Strasse 1, D-85740 Garching, Germany*
(Received 12 April 1994)

The breathing-mode giant monopole resonance (GMR) is studied within the framework of the relativistic mean-field (RMF) theory using the generator coordinate method (GCM). The constrained incompressibility and the excitation energy of isoscalar giant monopole states are obtained for finite nuclei with various sets of Lagrangian parameters. A comparison is made with the results of nonrelativistic constrained Skyrme Hartree-Fock (HF) calculations and with those from Skyrme random phase approximation (RPA) calculations. In the RMF theory the GCM calculations give a transition density for the breathing mode, which greatly resembles that obtained from the Skyrme HF+RPA approach and also that from the scaling mode of the GMR. From the systematic study of the breathing-mode as a function of the incompressibility in GCM, it is shown that the GCM succeeds in describing the GMR energies in nuclei and that the empirical breathing-mode energies of heavy nuclei can be reproduced by forces with an incompressibility close to $K = 300$ MeV in the RMF theory.

PACS number(s): 24.30.Cz, 21.60.Jz, 21.65.+f

I. INTRODUCTION

The nuclear matter incompressibility signifies an important and cardinal point on the equation of state (EOS). The behavior of the nuclear matter at the saturation point is relevant not only to the property of finite nuclei, but also to astrophysical phenomena such as supernovae explosion and neutron stars. The breathing-mode giant monopole resonance (GMR), whereby nuclei undergo radial density oscillations, provides a source for extracting the dynamical behavior, i.e., the compression properties of nuclei and nuclear matter [1]. In addition to the GMR excitation mode, which represents a small-amplitude collective motion, the intermediate energy heavy-ion collisions [2], on the other hand, strive to map out the EOS of the nuclear matter for densities higher than the saturation density. This is also expected to constrain the incompressibility at the saturation point. However, owing to the complex interplay of many degrees of freedom in the heavy-ion collision, it has not yet been possible to gain much insight into the behavior of the EOS. For properties around the saturation point, the GMR remains an important object of investigations.

The GMR has been measured over almost all of the Periodic Table [3]. Some time ago, the GMR energy was obtained [4] with considerable precision in a set of medium heavy Sn and Sm nuclei. Attempts were made to extract the nuclear matter incompressibility from such precision measurements. An earlier analysis based upon a leptodermous expansion of finite nuclear incompressibility into various finite-size components led to the nuclear matter incompressibility of 300 ± 25 MeV [5]. This analysis, which took into account the correlation of the Coulomb term involving the third derivative of the EOS, was based upon the systematics from the density-dependent Skyrme interactions. In a real case, however, Skyrme forces might not be reliable for this purpose. Circumventing this constraint based upon the Skyrme interactions, it was found that error bars on the nuclear matter incompressibility increased by more than 50% and the value itself was obtained at slightly higher than 300 MeV [6]. More recently an analysis of experimental data was attempted, including deformed nuclei and data from many laboratories [7]. However, this analysis, which again, comprises data of various origins, was not conclusive on the extraction of the nuclear matter incompressibility. A detailed and critical analysis of empirical breathing-mode GMR data is in progress.

Theoretically, the incompressibility has been obtained using the density-dependent interactions [8]. The deductions base themselves upon an interpolation between various Skyrme and Gogny forces for the GMR energies obtained from self-consistent Hartree-Fock and random phase approximation (HF+RPA) calculations. These calculations were a major effort intended to explaining the breathing-mode energies in finite nuclei in a microscopic approach. This approach, however, succeeded in reproducing the GMR energy of only ^{208}Pb within the interpolation scheme. The GMR energies of ^{90}Zr were overestimated by 1–2 MeV. This fact has been corroborated by the calculations within the RPA sum-rule approach using various Skyrme interactions [5]. The calculations

*Permanent address: Institute of Nuclear Research and Nuclear Energy, Bulgarian Academy of Sciences, Blvd. Tzarigradsko Chossee 72, Sofia 1784, Bulgaria.

indeed reproduce the GMR energy of ^{208}Pb using Skyrme force SkM*. The GMR energies of medium-heavy nuclei such as ^{90}Zr, Sn, and Sm isotopes could not, however, be reproduced within the Skyrme forces. The Skyrme interaction SkM* has been used extensively to calculate the properties of giant resonances [9]. It reproduces the empirical excitation energies of giant quadrupole resonance (GQR) very well. The appropriate effective mass of this force helps to achieve the required GQR energies. The force SkM*, however, reproduces the GMR energies of only ^{208}Pb well. This is due to a simple relationship of the surface incompressibility to the bulk incompressibility for the Skyrme type of forces, that for a given force the surface incompressibility has about the same value as the bulk incompressibility [10]. This relationship has essentially been at the root of the problems in describing adequately the mass dependence of the GMR energies in the Skyrme ansatz.

Relativistic mean-field (RMF) theory [11] has in the last years been found to be especially appealing in describing the ground-state properties of nuclei at and far away from the stability line [12,13]. The long-standing problem of the kink in isotope shifts in Pb nuclei, which could not be described with the Skyrme forces including all possible correlations, has been successfully solved in the RMF theory [14]. The theory has subsequently also been able to provide a good description of the binding energies and deformations of nuclei close to the neutron dripline [15]. Shell effects arising from the Dirac structure of the spin-orbit interaction in the RMF theory manifest in the behavior of the binding energies. The strong shell effects arising from the RMF theory are corroborated by the finite-range droplet model (FRDM) [16] and are in contrast with those from the Skyrme theory [17,18]. Thus, the RMF theory has achieved a considerable success in describing many aspects of the ground-state properties of nuclei.

The dynamical aspects within the RMF theory have remained largely unexplored. A first attempt was made to obtain the breathing-mode energies and incompressibilities within the RMF theory using the linear Walecka model in constrained calculations [19]. Such calculations were further extended to light nuclei, and anharmonicities in the breathing-mode oscillations were indicated [20]. The relationship of the GMR energies to the incompressibility of nuclear matter is, however, not yet known for the RMF theory. On the contrary, in the Skyrme approach, the relationship between the GMR energies and the incompressibility has been studied extensively (see, e.g., Refs. [8,10,5,1,9]) and has been found to be straightforward. An exercise to understand this relationship in the RMF theory has recently been undertaken [21], employing relativistic constrained calculations within the mean field. Another approach which has received considerable attention as a useful tool for studying properties of excited stated in nuclei is the generator coordinate method (GCM) [22]. It has been applied amongst others also for the breathing mode [23–25]. This has been attempted in the nonrelativistic theories with the intention of taking into account the relevant correlations in the nuclei. In this paper, we investigate the GCM for the first time in the RMF theory and focus upon the structure and properties of the breathing-mode GMR using the method of generator coordinates. A comparison of the properties of the GMR will be made with those from the Skyrme ansatz.

The paper is organized in the following way: In Sec. II we provide the theoretical framework of the RMF theory. The details on the generator coordinate method in the RMF theory are presented in Sec. III. The problem of the breathing mode GMR is discussed in Sec. IV. In Sec. V we discuss the results obtained in this framework. The last section contains a summary and conclusions.

II. RELATIVISTIC MEAN-FIELD THEORY

We start from relativistic mean field theory [11], which treats the nucleons as Dirac spinors ψ interacting by the exchange of several mesons: scalar σ meson that produces a strong attraction, isoscalar vector ω meson that causes a strong repulsion, isovector ρ meson required to generate the required isospin asymmetry, and photon that produces the electromagnetic interaction. The model Lagrangian density is:

$$\begin{aligned}\mathcal{L} = {} & \bar{\psi}\{i\gamma_\mu\partial^\mu - M\}\psi + \frac{1}{2}\partial^\mu\sigma\partial_\mu\sigma - U(\sigma) - g_\sigma\bar{\psi}\sigma\psi \\ & -\frac{1}{4}\Omega^{\mu\nu}\Omega_{\mu\nu} + \frac{1}{2}m_\omega^2\omega_\mu\omega^\mu - g_\omega\bar{\psi}\gamma_\mu\omega^\mu\psi \\ & -\frac{1}{4}\vec{R}^{\mu\nu}\vec{R}_{\mu\nu} + \frac{1}{2}m_\rho^2\vec{\rho}_\mu\vec{\rho}^\mu - g_\rho\bar{\psi}\gamma^\mu\vec{\tau}\psi\vec{\rho}_\mu \\ & -\frac{1}{4}F^{\mu\nu}F_{\mu\nu} - e\bar{\psi}\gamma^\mu\frac{(1-\tau_3)}{2}\psi A_\mu, \end{aligned} \tag{1}$$

where $U(\sigma)$ is the nonlinear scalar self-interaction with the cubic and quartic terms required for appropriate surface properties [26]:

$$U(\sigma) = \frac{1}{2}m_\sigma^2\sigma^2 + \frac{1}{3}g_2\sigma^3 + \frac{1}{4}g_3\sigma^4. \tag{2}$$

M, m_σ, m_ω, and m_ρ are the nucleon, the σ-, the ω-, and the ρ-meson masses, respectively, and g_σ, g_ω, g_ρ, and $e^2/4\pi$=1/137 are the coupling constants for the σ, ω, and the ρ mesons, and for the photon. The field tensors for the vector mesons are

$$\Omega^{\mu\nu} = \partial^\mu\omega^\nu - \partial^\nu\omega^\mu, \tag{3}$$

$$\vec{R}^{\mu\nu} = \partial^\mu\vec{\rho}^\nu - \partial^\nu\vec{\rho}^\mu - g_\rho(\vec{\rho}^\mu \times \vec{\rho}^\nu), \tag{4}$$

and for the electromagnetic field

$$F^{\mu\nu} = \partial^\mu A^\nu - \partial^\nu A^\mu. \tag{5}$$

The associated Hamiltonian operator $\hat{H}$ is then obtained using the well-known canonical quantization procedure based on the anticommutator (for the fermions) and the commutator (for the mesons) relations [27,28].

Within the relativistic mean-field (RMF) approximation the A-independent nucleons with single-particle spinors ψ_i $(i = 1, 2, ..., A)$, are assumed to form a single

Slater determinant Φ and to move independently in the meson fields. In the particular case of spherical nuclei, symmetries simplify the calculations considerably and only the timelike components $\omega^0(r)$, $\rho^0(r)$, and $A^0(r)$ of the ω, the ρ, and the electromagnetic fields survive. When describing ground-state properties of nuclei, one looks for static field solutions $\phi(r) = \sigma(r)$, $\omega^0(r)$, $\rho^0(r)$, and $A^0(r)$ that satisfy the Klein-Gordon equation

$$\left(-\frac{\partial^2}{\partial r^2} - \frac{2}{r}\frac{\partial}{\partial r} + m_\phi^2\right)\phi(r) = s_\phi(r), \tag{6}$$

where m_ϕ are the meson masses for $\phi = \sigma$, ω, ρ; m_ϕ is zero for the photon. The source terms

$$s_\phi(r) = \begin{cases} -g_\sigma\rho_s(r) - g_2\sigma^2(r) - g_3\sigma^3(r) & \text{for the } \sigma \text{ field} \\ g_\omega\rho_v(r) & \text{for the } \omega \text{ field} \\ g_\rho\rho_3(r) & \text{for the } \rho \text{ field} \\ e\rho_p(r) & \text{for the Coulomb field,} \end{cases} \tag{7}$$

depend on the spherical densities

$$\begin{aligned} \rho_s(r) &= \sum_{i=1}^{A} \bar{\psi}_i(\mathbf{r})\psi_i(\mathbf{r}) \\ \rho_v(r) &= \sum_{i=1}^{A} \psi_i^\dagger(\mathbf{r})\psi_i(\mathbf{r}) \\ \rho_3(r) &= \sum_{i=1}^{A} \psi_i^\dagger(\mathbf{r})\tau_3\psi_i(\mathbf{r}) \\ \rho_p(r) &= \sum_{i=1}^{A} \psi_i^\dagger(\mathbf{r})\frac{(1-\tau_3)}{2}\psi_i(\mathbf{r}), \end{aligned} \tag{8}$$

where, in the no-sea approximation, the summation runs over all occupied states in the Slater determinant Φ. The solution of Eq. (6) can, in principle, be expressed in terms of Green's functions, i.e.,

$$\phi(r) = \int_0^\infty G_\phi(r,r')s_\phi(r')r'^2dr', \tag{9}$$

where, for the massive fields,

$$G_\phi(r,r') = \frac{1}{2m_\phi}\frac{1}{rr'}\left(e^{-m_\phi|r-r'|} - e^{-m_\phi|r+r'|}\right), \tag{10}$$

and for the Coulomb field,

$$G_\phi(r,r') = \begin{cases} 1/r & \text{for } r > r' \\ 1/r' & \text{for } r < r'. \end{cases} \tag{11}$$

The total ground-state energy of spherical nuclei can be expressed, in the center-of-mass frame, as a functional of the baryon spinors $\{\psi_i\}$

$$E_{\mathrm{RMF}}[\psi_i] \equiv \langle\Phi|\hat{H}|\Phi\rangle, \tag{12}$$

where the Hamiltonian density

$$\begin{aligned} \mathcal{H}_{\mathrm{RMF}}(r) = \tau(r) &+ M\rho_s(r) + \tfrac{1}{2}g_\sigma\rho_s(r)\sigma(r) \\ &- \tfrac{1}{2}\{\tfrac{1}{3}g_2\sigma^3(r) + \tfrac{1}{2}g_3\sigma^4(r)\} \\ &+ \tfrac{1}{2}g_\omega\rho_v(r)\omega^0(r) + \tfrac{1}{2}g_\rho\rho_3(r)\rho^0(r) \\ &+ \tfrac{1}{2}e\rho_p(r)A^0(r) \end{aligned} \tag{13}$$

depends only on the baryon field since the "kinetic" energy density

$$\tau(r) \equiv \sum_{i=1}^{A} \psi_i^\dagger(\mathbf{r})\{-i\boldsymbol{\alpha}\boldsymbol{\nabla}\}\psi_i(\mathbf{r}) \tag{14}$$

and the spherical densities (8) and therefore the mesonic fields (9) are all expressed in terms of the Dirac spinors $\{\psi_i\}$. In the RMF approach, Fock terms in Eq. (13) are neglected.

Taking the variation of Eq. (12) with respect to $\psi_i^\dagger$ one obtains the stationary Dirac equation with the single-particle energies as eigenvalues,

$$\hat{h}_D\psi_i(\mathbf{r}) = \varepsilon_i\psi_i(\mathbf{r}), \tag{15}$$

where

$$\begin{aligned} \hat{h}_D = &-i\boldsymbol{\alpha}\boldsymbol{\nabla} + \beta(M + g_\sigma\sigma(r)) \\ &+ g_\omega\omega^0(r) + g_\rho\tau_3\rho^0(r) + e\frac{(1-\tau_3)}{2}A^0(r). \end{aligned} \tag{16}$$

Solving this equation self-consistently [the mesonic fields depend on the baryon solution according to Eq.(9)], one obtains the nuclear ground state Φ_0 in terms of the solutions $\{\psi_i\}$.

III. RELATIVISTIC GENERATOR COORDINATE METHOD

The GCM has been used extensively within the non-relativistic approaches to obtain the ground state and excited states of nuclei [29]. With the use of the Skyrme forces, the GCM was applied to study the giant resonances [24]. Recently, the GCM has also been employed to investigate the effect of correlations on the ground-state properties of nuclei [30]. Here we present a relativistic extension of the generator coordinate method (GCM), which is based upon a trial A-particle wave function ansatz Ψ_{GCM} written in the form of a linear combination:

$$\Psi_{\mathrm{GCM}}(\mathbf{r}_1,\ldots,\mathbf{r}_A) = \int \mathcal{F}(q)\Phi(\mathbf{r}_1,\ldots,\mathbf{r}_A;q)dq, \tag{17}$$

where the generating function $\Phi(q) \equiv \Phi(\mathbf{r}_1,\ldots,\mathbf{r}_A;q)$ is

chosen to be a Slater determinant $\Phi(q)$ built upon single-particle spinors $\psi_i(\mathbf{r},q),(i=1,2,...,A)$, depending on the generator coordinate q. It is obvious that in this case the wave function of the system (17), being a superposition of Slater determinants $\Phi(q)$, goes beyond the limits of the RMF approach. The so-called "weight," or "generator" function $\mathcal{F}(q)$ is determined after varying with respect to $\mathcal{F}(q)$ the energy of the system

$$E[\mathcal{F}]=\frac{\langle\Psi_{\rm GCM}|\hat{H}|\Psi_{\rm GCM}\rangle}{\langle\Psi_{\rm GCM}|\Psi_{\rm GCM}\rangle}. \tag{18}$$

This leads to the Hill-Wheeler integral equation for the weight function:

$$\int[\mathcal{H}(q,q')-E\mathcal{N}(q,q')]\,\mathcal{F}(q')dq'=0, \tag{19}$$

where

$$\mathcal{H}(q,q')=\langle\Phi(q)|\hat{H}|\Phi(q')\rangle \tag{20}$$

and

$$\mathcal{N}(q,q')=\langle\Phi(q)|\Phi(q')\rangle \tag{21}$$

are the energy and the norm overlap kernels, respectively.

A straightforward calculation shows that with the Hamiltonian $\hat{H}$ associated with our model Lagrangian (1) one obtains

$$\mathcal{H}(q,q')\equiv\langle\Phi(q)|\hat{H}|\Phi(q')\rangle, \tag{22}$$

where $\mathcal{N}(q,q')$ is the overlap kernel (21) and $\mathcal{H}(r;q,q')$ is the overlap energy-density kernel:

$$\begin{aligned}\mathcal{H}(r;q,q')=&\tau(r;q,q')+M\rho_s(r;q,q')+\tfrac{1}{2}g_\sigma\rho_s(r;q,q')\sigma(r;q,q')\\&-\tfrac{1}{2}\{\tfrac{1}{3}g_2\sigma^3(r;q,q')+\tfrac{1}{2}g_3\sigma^4(r;q,q')\}+\tfrac{1}{2}g_\omega\rho_v(r;q,q')\omega^0(r;q,q')\\&+\tfrac{1}{2}g_\rho\rho_3(r;q,q')\rho^0(r;q,q')+\tfrac{1}{2}e\rho_p(r;q,q')A^0(r;q,q').\end{aligned} \tag{23}$$

In this equation the "kinetic" energy density is defined by the spinors $\{\psi_i(\mathbf{r};q)\}$ as

$$\tau(r;q,q')=\sum_{i,j=1}^{A}N_{ji}^{-1}\,\psi_i^\dagger(\mathbf{r};q)\{-i\boldsymbol{\alpha}\boldsymbol{\nabla}\}\psi_j(\mathbf{r};q'). \tag{24}$$

Similarly the other densities entering Eq. (23) are

$$\begin{aligned}&\rho_s(r;q,q')=\sum_{i,j=1}^{A}N_{ji}^{-1}\,\bar{\psi}_i(\mathbf{r};q)\psi_j(\mathbf{r};q'),\quad \rho_v(r;q,q')=\sum_{i,j=1}^{A}N_{ji}^{-1}\,\psi_i^\dagger(\mathbf{r};q)\psi_j(\mathbf{r};q'),\\&\rho_3(r;q,q')=\sum_{i,j=1}^{A}N_{ji}^{-1}\,\psi_i^\dagger(\mathbf{r};q)\tau_3\psi_j(\mathbf{r};q'),\quad \rho_p(r;q,q')=\sum_{i,j=1}^{A}N_{ji}^{-1}\,\psi_i^\dagger(\mathbf{r};q)\frac{(1-\tau_3)}{2}\psi_j(\mathbf{r};q').\end{aligned} \tag{25}$$

They appear as source terms

$$s_\phi(r;q,q')=\begin{cases}-g_\sigma\rho_s(r;q,q')-g_2\sigma^2-g_3\sigma^3 & \text{for the }\sigma\text{ field}\\ g_\omega\rho_v(r;q,q') & \text{for the }\omega\text{ field}\\ g_\rho\rho_3(r;q,q') & \text{for the }\rho\text{ field}\\ e\rho_p(r;q,q') & \text{for the Coulomb field,}\end{cases} \tag{26}$$

in Klein-Gordon equations of the type (6) whose solution determines the fields $\phi(r;q,q')=\sigma(r;q,q')$, $\omega^0(r;q,q')$, $\rho^0(r;q,q')$ and $A^0(r;q,q')$ entering Eq. (23) as

$$\phi(r;q,q')=\int_0^\infty G_\phi(r,r')s_\phi(r';q,q')r'^2dr'. \tag{27}$$

The Green functions are defined as before by Eqs. (10) and (11).

In the above equations the sums run over all occupied single-particle states and N_{ij}^{-1} are the elements of the matrix $N^{-1}(q,q')$ where

$$N_{ij}(q,q')=\int d^3r\,\psi_i^\dagger(\mathbf{r};q)\psi_j(\mathbf{r};q'). \tag{28}$$

The determinant of $N(q,q')$ simply gives the overlap kernel (21)

$$\mathcal{N}(q,q')=\det\{N(q,q')\}. \tag{29}$$

Thus, having determined the integral kernels (22) and (29), the associated Hill-Wheeler integral equation (19) has to be solved in order to determine the nuclear ground and n-excited states through its eigensolutions $\{E_0,\mathcal{F}_0(q)\}$ and $\{E_n,\mathcal{F}_n(q)\}$, respectively.

IV. ISOSCALAR GIANT MONOPOLE RESONANCE

The constrained Hartree-Fock calculations have been a common method to obtain description of the excited

states in nuclei. An extension of this method in the framework of the RMF theory has been made recently, where the breathing-mode GMR in finite nuclei has been obtained in the constrained calculations [21]. We extend some of the discussion here for the sake of clarity. In order to analyze the isoscalar GMR we perform also constrained RMF calculations, where the Dirac equation [see Eq. (15)]

$$(\hat{h}_D - qr^2)\psi_i(x) = \varepsilon_i\psi_i(x) \tag{30}$$

is solved at different values of the Lagrange multiplier q which are associated with values of the nuclear root-mean-square (rms) radius

$$R = \left\{\frac{1}{A}\int r^2\rho_v(r;q)d^3r\right\}^{1/2}, \tag{31}$$

where

$$\rho_v(r;q) = \sum_{i=1}^{A}\psi_i^\dagger(\mathbf{r};q)\psi_i(\mathbf{r};q) \tag{32}$$

is the baryon local density determined by the solution $\{\psi_i(\mathbf{r};q)\}$. According to Eq. (12), the total energy of the constrained system

$$E_{\rm RMF}(q) = E_{\rm RMF}[\psi_i(q)] \tag{33}$$

is a function of q (or the nuclear rms radius R). It has a minimum, the ground-state energy $E^0_{\rm RMF} = E_{\rm RMF}(0)$, at $q = 0$ corresponding to the ground-state rms radius R_0. The curvature of this function around the equilibrium point R_0 defines the so-called constrained incompressibility coefficient of the finite nucleus

$$K_C(A) = A^{-1}\left(R^2\frac{d^2E_{\rm RMF}(q)}{dR^2}\right)_{q=0}. \tag{34}$$

The constrained energy (33) as a function of q represents the energy surface for the isoscalar monopole motion of the nucleus, where R changes around its ground-state value R_0. In order to derive vibrational excitation energies one needs in addition the inertial parameter for this motion. In the nonrelativisitic RPA sum-rule approach (SRA) [31], the inertia parameter for the GMR is derived as MR_0^2. In this case one obtains the GMR excitation energy E_1 as

$$E_1 = \sqrt{\frac{K_C(A)}{MR_0^2}}. \tag{35}$$

In order to obtain a description of the GMR in the RMF theory, we consider the Lagrange multiplier q entering Eq. (30) as generator coordinate for the GCM calculations as described in Sec. III. The solution $\{\psi_i(\mathbf{r};q)\}$ of Eq.(30) at different values q then defines the generator Slater determinants $\Phi(q)$ and therefore the integral kernels (20) and (21). In fact, the diagonal part of the energy kernel $\mathcal{H}(q,q')$ coincides with the constrained energy (33), i.e., $E_{\rm RMF}(q) \equiv \mathcal{H}(q,q)$. The off-diagonal elements $\mathcal{H}(q,q')$ contain the information about the inertia. We then solve the resulting Hill-Wheeler equation (19) numerically using the method of Ref. [24].

V. RESULTS

A. Relativistic GCM calculations

We have performed GCM calculations for four closed-shell nuclei ^{16}O, ^{40}Ca, ^{90}Zr, and ^{208}Pb with the sets of Lagrangian parameters given in Table I. The Lagrangian parameters sets are NL1 [32], NL-SH [13], NL2 [33], HS [34], and L1 [33] in the increasing order of the nuclear matter incompressibility with $K_{\rm NM}$ = 211.7, 355.0, 399.2, 545, and 626.3 MeV, respectively. This allows us to examine the dependence of GMR energies on the nuclear matter incompressibility $K_{\rm NM}$. These sets of parameters have also been employed in our earlier constrained RMF calculations [21]. The last two sets, HS and L1, correspond to the linear model without the self-coupling of the σ field. In addition, the set L1 excludes the contri-

TABLE I. Parameter sets for the Lagrangian (1).

	NL1 [32]	NL-SH [13]	NL2 [33]	HS [34]	L1 [33]
M[a]	938.0	939.0	938.0	939.0	938.0
m_σ	492.25	526.0592	504.89	520.0	550.0
m_ω	795.355	783.0	780.0	783.0	783.0
m_ρ	763.0	763.0	763.0	770.0	
g_σ	10.138	10.44355	9.111	10.47	10.30
g_ω	13.285	12.9451	11.493	13.80	12.60
g_ρ	4.975	4.3828	5.507	4.04	
g_2	−12.172	− 6.9099	−2.304	0.0	0.0
g_3	−36.265	−15.8337	13.783	0.0	0.0
		Nuclear matter characteristics			
M^*/M	0.57	0.60	0.67	0.54	0.53
$K_{\rm NM}$	211.7	355.0	399.2	545.0	626.3
$a_{\rm sym}$	43.5	36.1	43.9	35.0	

[a]The masses, the incompressibility K_{NM} and the asymmetry energy $a_{\rm sym}$ are in MeV; the coupling g_3 is in fm^{-1}.

bution from the ρ field. Among the sets NL1, NL-SH, and NL2, which correspond to the nonlinear model, only the set NL2 has a positive coupling constant g_3 in Eq. (2). The set NL2 has an effective mass $m^* = 0.67$ at the saturation, which is higher than that of NL1 and NL-SH. Whereas the set NL1 reproduces the ground-state properties of nuclei only close to the stability line due to the very large asymmetry energy, the set NL-SH describes also nuclei far away from the stability line [13]. The shell effects at the drip line and deformation properties obtained with NL-SH have been found to be in good agreement with the recent finite-range droplet model [16]. In order to cover the region of the incompressibility about 300 MeV, we have also constructed a schematic force NL-S1 with $K_{\rm NM} = 296$ MeV. This force describes the ground-state properties of closed-shell nuclei rather well, but has a large asymmetry energy of 52 MeV. The use of various parameter sets in our GCM calculations allows us to study the influence of the model Lagrangian and their properties on the properties of the GMR energies. The aim of the present study is also to examine how the GCM works in the RMF theory.

The self-consistent solution of the constrained mean field problem (30) diverges for large positive and negative values of the constraining parameter q. For large positive values the quadratic r dependence of the constraining operator leads to unbound solutions. For large negative values of q, when the nuclear rms radius R decreases, the self-consistent mean-field potential pushes up the single-particle energies and the RMF solution disappears at some minimal rms radius $R_{\rm min}$. The instability for negative q values causes no further problems. For positive q, however, we find only a very limited range of possible q values close to the ground state. We therefore introduce a cutoff function $[1+\exp(r-R_{\rm cut}/a)^{-1}]$ multiplying r^2 in the constrained RMF calculations. The cutoff radius was chosen to be $R_{\rm cut} = 2r_0A^{1/3}$ with $r_0 = 1.2$ fm. The diffuseness parameter was set at $a = 0.5$ fm. In Fig. 1 we show the first three excited states for ^{90}Zr obtained in the relativistic GCM calculations with the force NL-SH. The effect of the cutoff function is demonstrated in this figure by two constrained RMF calculations, one with (dot-dash line) and the other without (solid line) the cutoff function. The GCM kernel without cutoff goes only up to 4.35 fm on the right side of the ground state as shown by the solid curve. It can be seen that the inclusion of the cutoff function enlarges the required space for the GCM calculations without changing the behavior of the integral kernels beyond the one calculated without the cutoff function.

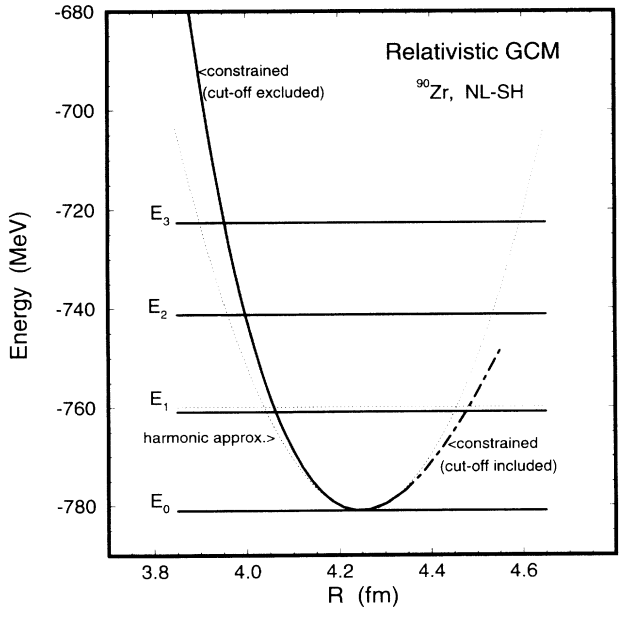

FIG. 1. The constrained energy Eq. (33) as a function of the rms radius R in Eq. (31), for ^{90}Zr with the force NL-SH in the GCM calculations. The solid curve on the left is without taking the cut-off function into account. For the lower densities (higher R) the constrained energy has been extended (dot-dash line) by inclusion of the cut-off function. The harmonic approximation to the curve is shown by the dotted parabola. The energies of the first three excited states (E_1, E_2, and E_3) along with the ground-state energy E_0 are also shown. The energy E_1 in the harmonic approximation (dotted line) differs only slightly from the actual value.

B. The correlated ground state

Solving the Hill-Wheeler equation (19) we obtain the weight function $g_0 = \mathcal{N}^{1/2}\mathcal{F}_0$ associated with the ground-state solution $\mathcal{F}_0(q)$. Functions $g_0(q)$ show the

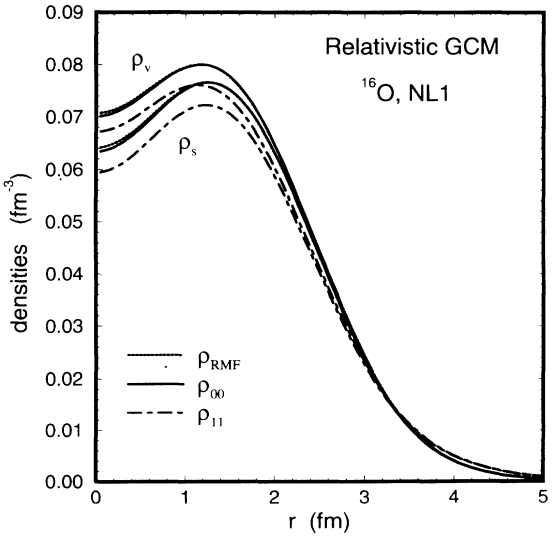

FIG. 2. The ground-state vector and scalar densities for protons in the RMF ($\rho_{\rm RMF}$) and in the GCM (ρ_{00}) for ^{16}O. The effect of the ground-state correlations in the GCM densities are seen to be minimal. The GCM density for the first excited state of the GMR (ρ_{11}) is also shown, where there is a considerable change in the densities in the interior. A slight change in the surface of the nucleus can also be seen.

TABLE II. RMF and constrained GCM results for the ground-state energies and mass rms radii and for the excitation energies $\Delta E_n = (E_n - E_0)$ of the first three monopole states calculated with the set NL1.

Nuclei	Energies (MeV)		Radii (fm)		Excitation energies (MeV)		
	RMF	GCM	RMF	GCM	ΔE_1	ΔE_2	ΔE_3
^{16}O	−127.2	−127.5	2.65	2.65	20.6	38.9	49.8
^{40}Ca	−342.5	−342.6	3.38	3.38	17.1	29.9	37.3
^{90}Zr	−784.9	−785.0	4.28	4.28	14.7	29.1	43.1
^{208}Pb	−1639.9	−1640.1	5.67	5.67	11.7	23.3	34.9

usual bell shape with a maximum around the RMF ground-state value q=0. With an increase in mass number A the width of $g_0(q)$ decreases, while its amplitude increases keeping fixed the normalization $\mathcal{FNF} = 1$.

Typical GCM results for energies and rms radii calculated with the set NL1 are given in Table II. It is worth noting that the GCM ground-state energy is slightly lower than the RMF one. This small difference, which is too small to be seen in Fig. 1, contains in fact two contributions: (i) the positive zero-point energy of roughly $1/2\hbar\omega$ in the harmonic approximation and (ii) the correlation energy induced by the GCM correlations lowering the mean field energy of the ground state by roughly the same amount. This is an important point and reflects the fact that GCM is beyond the RMF approximation.

There is also no perceptible effect on the rms radii of the nuclear ground state in the GCM. The largest difference between the RMF and the GCM ground-state rms radii is seen for the nucleus ^{16}O. It is about 0.0025 fm. Figure 2 shows the RMF and the GCM vector (ρ_v) and scalar (ρ_s) densities. The RMF and GCM local densities do not differ significantly. For heavy nuclei the GCM ground-state local densities are even closer to the uncorrelated RMF ones. We can thus conclude that the correlations in the GCM ground state are small and the main purpose of the GCM consideration here is in the possibility of its generating nuclear excited states.

C. GMR excited states

The first three GMR excited states obtained in the GCM with the parameter set NL1 are shown in Table II. These states show a clear equidistant spectrum for heavy nuclei. A similar behavior is also apparent from Fig. 1 for ^{90}Zr too, which has been shown for the set NL-SH. For the lighter nuclei, however, there are significant deviations from this type of spectrum, as can be seen from the energies of the excited states in ^{40}Ca and ^{16}O. With an increase in mass number, the excitation energies decrease. Here we take the excitation energy $\Delta E_1 = E_1 - E_0$, which is equivalent to the excitation energy of a collective state in the nonrelativistic constrained Hartree-Fock approach. The mass dependence $\Delta E_1 = cA^{-1/3}$ of the excitation energy for ^{208}Pb, the nucleus on which there exists well-measured GMR energy, is obtained as c = 69.1, 79.6, 93.6, 104.9, 97.0, and 126.2 MeV for the sets NL1, NL-S1, NL-SH, NL2, HS, and L1, respectively.

In Fig. 2 we show the local vector and scalar densities $\rho_{00}(r)$ of the GCM ground state and $\rho_{11}(r)$ of the first excited GMR state for the set NL1. The densities are more extended in space in comparison with the ground-state ones. Consequently, the rms radii in the first exited state are larger than that of the associated ground-state values by about 0.15 fm in ^{16}O and by only 0.015 fm in ^{208}Pb.

D. Transition density

The transition density of the GMR provides the strongest evidence for the radial density oscillations in nuclei and hence of the "breathing" or the compression character of the GMR mode. We show in Fig. 3 the vector and scalar transition densities $\rho_{01}(r)$ for protons and neutrons in ^{208}Pb obtained in the relativistic GCM calculations for the force NL-SH. The transition densities show a change in the density in the bulk at the expense of that in the surface. A node at 6 fm is clearly to be seen for protons and at about 6.4 fm for neutrons. The existence of a well-defined node in the transition density is the typical behavior for the breathing-mode motion and testifies for the compressional property of the GMR. The

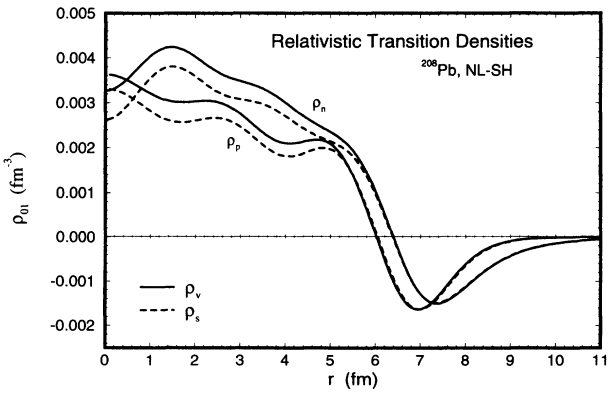

FIG. 3. The vector and the scalar transition density for the GMR in ^{208}Pb obtained in the relativistic GCM calculations with the force NL-SH. There is a conspicuous node in the densities of both the protons and neutrons. The change in the bulk of the vector density takes place at the expense of the change in the surface, thus conserving the total number of particles.

transition density from RPA calculations for the GMR in ^{208}Pb with Skyrme force SIII was seen to be very similar to the transition density in Fig. 3. The transition density for SIII also showed a node at about 6.2 fm. Both these transition densities, one in the RMF theory for NL-SH and the other in the Skyrme approach for SIII, closely resemble that obtained from a simple radial scaling of ground-state density. The point of difference to be noted is that in our RMF case, we have obtained the transition density for the GMR in the GCM, with some form of a constrained motion. Here we do not observe any conspicuous differences between the transition densities of the relativistic GCM and the scaling mode in the Skyrme approach. The oscillations in the interior of the nucleus are obviously due to the shell effects. The vector transition density shown in the figure conserves the particle number. The same cannot, however, be said for the scalar transition density, which is albeit similar to the vector transition density, but manifests mainly the relativistic effect similar to that exhibited by total scalar density.

We observe that the difference between the scalar and the vector transition densities, which is connected with the small components of the Dirac wave functions, arises mainly in the interior of the nucleus. In the surface region both densities coincide more or less.

E. Constrained incompressibility of finite nuclei

We now consider the constrained incompressibility $K_C(A)$ as calculated from Eq. (34). The results as a function of the nuclear matter incompressibility $K_{\rm NM}$ are shown in Fig. 4 for a few nuclei. It may be worth mentioning that empirically the GMR has been well established only in heavy nuclei such as ^{208}Pb and ^{90}Zr. We have also included the light nuclei such as ^{40}Ca, ^{16}O, and ^{4}He. In the light nuclei it is very uncertain and a full energy-weighted sum-rule strength has rarely been observed. Thus, in our case the light nuclei serve mostly the purpose of illustration and for the possible anharmonic effects.

With exceptions for light nuclei, the incompressibility $K_C(A)$ shows a strong dependence on the nuclear matter incompressibility $K_{\rm NM}$. For the linear force HS, $K_C(A)$ shows a slight dip from the increasing trend for ^{208}Pb and ^{90}Zr, whereas for light nuclei ^{40}Ca, ^{16}O, and ^{4}He, the HS values are even smaller than the NL2 values. The dependence of $K_C(A)$ in the Skyrme approach is different, where it increases monotonically with $K_{\rm NM}$. The finite nuclear incompressibility receives a sizeable contribution from the surface incompressibility, and this difference could be explained from the difference in the behavior of the surface incompressibility in the two methods. In the Skyrme approach, the surface incompressibility has been shown to be $K_S \sim -K_{NM}$ for all standard Skyrme forces. This does not seem to be the case for the RMF theory, however, as shown by the HS values. Thus, the surface incompressibility is not necessarily a straight function of the nuclear matter incompressibility in the RMF theory. This point has also been dealt with in Ref. [21].

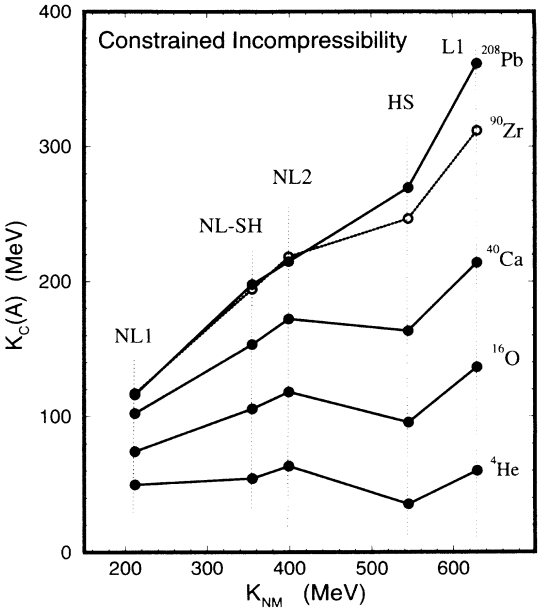

FIG. 4. The constrained incompressibility K_C obtained in the RMF theory using various parameter sets. K_C increases monotonically from NL1 to NL-SH for all nuclei. The values for HS show a slight dip, indicating a very large surface incompressibility.

F. Comparison with nonrelativistic calculations and experimental data

The excitation energy ΔE_1 corresponds to the energy $E^{(1)}$ usually obtained from the nonrelativistic constrained Skyrme Hartree-Fock (SHF) calculations within the sum rule approach [10]. In Table III, energies ΔE_1 are compared with such nonrelativistic constrained SHF results obtained with the Skyrme-type forces SkM and SIII. These Skyrme forces have nearly the same nuclear matter incompressibility $K_{\rm NM}$ as do the sets NL1 and NL-SH, respectively. It can be seen that the nonrelativistic SHF results differ slightly from the values of ΔE_1. This difference in the relativistic GCM excitation energy ΔE_1 from the SHF energy is small for heavy nuclei. It, however, increases for lighter nuclei, where the GCM shows lower values.

Figure 5 shows the GCM breathing-mode energy ΔE_1 for various nuclei and parameter sets. The energy ΔE_1 first increases with $K_{\rm NM}$ from NL1 to NL2 almost linearly for all nuclei. For the force HS, which has $K_{\rm NM}$ even larger than that of NL2, the energy shows a decrease for all the nuclei, however. This is due to a rather large surface incompressibility which is in disproportion to its bulk incompressibility for HS. This reduces the incompressibility of the nuclei, as also shown in Fig. 4. For the force L1, ΔE_1 shows an increase compared to HS. Thus, ΔE_1 is not related in a simple way to $K_{\rm NM}$. This reflects the role played by the surface component of the compression in the RMF theory. Even for heavy nuclei ΔE_1 does not show an overall increasing tendency with $K_{\rm NM}$. For lighter nuclei this effect is even more

TABLE III. Comparison of the GMR excitation energies (in MeV) obtained within the constrained GCM calculations and the approximation (35) using the constrained incompressibility (34) with the nonrelativistic sum-rule approach obtained within nonrelativistic constrained Hartree-Fock (HF) calculations [31]. In the relativistic case sets NL1 and NL-SH are used, which have nearly the same nuclear matter incompressibility K_{NM} as do the sets of Skyrme force parameters SkM and SIII used in the nonrelativistic HF calculations [11].

	NL1: K_{NM} = 211.7 MeV SkM: K_{NM} = 216.7 MeV			NL-SH: K_{NM} = 354.95 MeV SIII: K_{NM} = 356.00 MeV		
Nuclei	GCM	Eq. (35)	Skyrme HF	GCM	Eq. (35)	Skyrme HF
^{16}O	20.6	20.9	22.4	25.3	25.8	26.6
^{40}Ca	17.1	19.2	20.2	22.4	23.9	24.7
^{90}Zr	14.7	16.3	17.0	20.16	21.1	21.2
^{208}Pb	11.7	12.2	12.9	15.8	16.1	16.2

apparent.

It is interesting to note that the dip in energy ΔE_1 for HS seems to signal the transition from nonlinear (NL1, NL-SH, NL2) to linear (HS, L1) models in the Lagrangian (1). Even with significantly higher nuclear matter incompressibility (K_{NM}= 545 MeV for HS) the linear model gives comparable GMR excitation energies (and even lower) in comparison with the nonlinear ones (notice that K_{NM}= 399.2 MeV for NL2).

It is instructive to see that the approximate expression, (35) which is exactly the same as in the nonrelativistic sum-rule approach but calculated with the incompressibility $K_C(A)$ emerging from the relativistic RMF calculations, gives acceptable results for GMR excitation energies. The results from Eq. (35) are compared with the GCM and SHF results also in Table III.

In the nonrelativistic approach using density-dependent interactions, extensive work was carried out to obtain the incompressibility and breathing-mode energy [8] with HF + RPA calculations. The RPA calculations were performed on a set of Skyrme and Gogny interactions including the finite-range Gogny force D1, with an increasing order of incompressibility of nuclear matter. This work attempted to reproduce the empirical breathing-mode energies on ^{208}Pb and ^{90}Zr, where experiments showed the existence of the GMR unambiguously. The GMR energy in ^{208}Pb is rather well established and lies at 13.7±0.3 MeV. The GMR energy in ^{90}Zr has been measured to be in the range 16.5 – 17.3 MeV by different experiments. The average value of the energy from different experiment comes at about 17.0 MeV. Table IV shows the GMR values for ^{90}Zr and ^{208}Pb obtained in the RPA calculations [8] for the forces D1, Ska, and SIII. A comparison of the RPA values with the empirical values in Table IV shows that the Gogny force D1 reproduces the GMR energy for ^{208}Pb quite well. The force D1, however, overestimates the GMR energy for ^{90}Zr by about 1.5 MeV. The force Ska, which has incompressibility of nuclear matter at 263 MeV, gives the GMR energy for ^{208}Pb only slightly higher than D1. The GMR energy with Ska for ^{90}Zr is, however, about 2 MeV higher than the empirical value. Thus, within the nonrelativistic approach, with D1 one comes very close to reproducing the GMR energy of ^{208}Pb in the RPA calculations. The GMR energy of ^{90}Zr could not, however, be reproduced by any Skyrme force. This has been the scenario within the Skyrme approach, where the conclusions of Ref. [8] on the incompressibility hinged very strongly on ^{208}Pb only. Consequently, a value of the incompressibility of nuclear

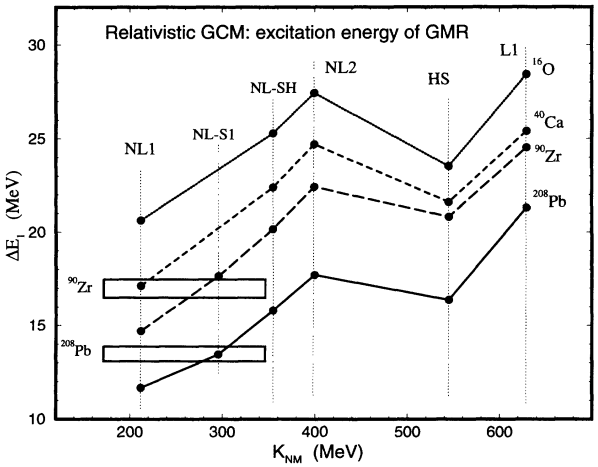

FIG. 5. The energy ΔE_1 of the GMR obtained with various relativistic Lagrangian sets in the GCM. The empirical values of the GMR in ^{208}Pb and ^{90}Zr have been shown at their average values by horizontal quadrangles. The widths of the quadrangles span the error bars in the empirical data. The empirical data encompass the corresponding GCM results at about K = 280 – 310 MeV and show a good agreement with the values obtained with the set NL-S1.

TABLE IV. Comparison of the RMF results from the parameter set NL-S1, with the HF+RPA calculations using density-dependent Skyrme interactions. Here we show the results only for the nuclei ^{208}Pb and ^{90}Zr, where the empirical data is reliable and rather well established.

	Skyrme interactions+RPA			GCM-RMF	
	D1	Ska	SIII	NL-S1	Expt.
K_{NM}	228	263	356	296	
^{90}Zr	18.5	19.1	22.1	17.6	17.0 ± 0.5
^{208}Pb	14.4	14.7	17.2	13.4	13.5 ± 0.3

matter of about 210 MeV seem to have been favoured.

We now compare the empirical values and the RPA results with those in the relativistic GCM calculations with the force NL-S1. It may be noted that this force which describes the ground-state properties of nuclei only very approximately, and was constructed with a view to fill in the gap at about $K_{\rm NM} \sim 300$ MeV in the dependence of the incompressibility on the breathing-mode energy. It has presently only a schematic character. With its incompressibility of 296 MeV, the GMR energy for ^{208}Pb in the GCM has been obtained at 13.4 MeV. It is very close to the empirical values obtained in many experiments. The GCM energy for ^{90}Zr has been obtained at 17.6 MeV, which is slightly higher than the average value of 17.0 MeV but is closer to an earlier empirical result. On the whole, it is within the uncertainties of the empirical values. In comparison, the GMR energy from the Gogny force D1 in the RPA lies at 18.5 MeV. Systematics of the values for ^{208}Pb and ^{90}Zr in Fig. 5 show that both empirical values as shown by the quadrangles are encompassed by the GCM calculations curve from $K_{\rm NM} = 290 - 310$ MeV. The width of the quadrangles signify the corresponding experimental uncertainties in the determination of the GMR centroid energies. The empirical values themselves have been reproduced by $K_{\rm NM} \sim 300$ MeV as can be seen by intersecting the empirical values at the curves for ^{208}Pb and ^{90}Zr.

VI. CONCLUSIONS AND DISCUSSION

We have performed a systematic study of the breathing-mode energy and the incompressibility of finite nuclei with the generator coordinate method in the RMF theory. It has been observed that the transition density of the giant monopole mode shows a character very similar to that obtained in the Hartree-Fock–RPA approach with density-dependent Skyrme interactions. This behavior is also similar to what one expects in the simple radial scaling of the ground-state density.

Using a set of relativistic mean-field Lagrangian parameters, it has been shown that the GCM energies for the realistic forces show an increasing tendency with the nuclear matter incompressibility. Only for unrealistic forces such as HS does one observe a decrease in the breathing-mode energy and also in the incompressibility of nuclei even when this force has a larger $K_{\rm NM}$. This is due to a very large surface incompressibility of HS.

The GCM values obtained with the force NL1 are much lower than the empirical values, and those with NL-SH are a little higher than the latter. The empirical GMR energies, on the other hand, can be well encompassed by the GCM curve at $K = 280 - 310$ MeV. This is corroborated by the GCM values obtained with a rather schematic force having an incompressibility $K = 296$ MeV, where the GCM values for ^{208}Pb and ^{90}Zr are very close to the corresponding empirical values. Thus, the empirical GMR energies for both these nuclei have been clearly bracketed by the GCM calculations in the RMF theory. We know of no other theoretical result where the GMR energies for both these nuclei have been reproduced. Our results also bring about severe constraints on the value of the nuclear matter incompressibility, the observable which has theoretically been held rather uncertain. The GCM results, thus, favor an incompressibility at about 300 MeV. This is in contrast with the usual assumption of the incompressibility of about 210 MeV concluded from the nonrelativistic Skyrme ansatz, where the empirical value for ^{208}Pb only could be reproduced. Our conclusion, on the other hand, is in good agreement with the analysis of the empirical breathing-mode energies, where the incompressibility of nuclear matter was obtained as 300 MeV or higher [5,6]. This analysis is, however, not yet complete and further work on it is in progress.

Differences in the shell effects of the RMF theory and the Skyrme approach and their implications on the ground-state properties of nuclei such as isotope shifts [14] and on nuclei at drip lines [15] have been discussed earlier. The present work on the breathing-mode energies in the GCM has brought about important differences also in the dynamical properties of the RMF theory and the Skyrme ansatz. The nearly good reproduction of the empirical GMR energies in the relativistic GCM approach has become possible due to the ratio of the surface incompressibility to the bulk incompressibility, which has been obtained as different from 1 in the RMF forces. This was also demonstrated in Ref. [35] using various schematic parameter sets where, in the RMF theory, it is possible to obtain the ratio of the surface incompressibility to the bulk incompressibility of up to about 2 or more. For the realistic parameter sets NL1 and NL-SH, this ratio has been shown [21] to be higher than 1 (1.58 and 1.72, respectively) in the simple radial scaling of the ground-state density in the semi-infinite nuclear matter with the Thomas-Fermi approximation. In the Skyrme approach, the ratio of 1 has essentially been at the origin of problems in describing the mass dependence of the GMR energies. Of course, there still remain some improvements to be made in the ansatz of the RMF theory with a view to describe accurately the ground-state energies of nuclei at and far away from the stability line as is the case with the force NL-SH as well as the dynamical properties such as the breathing-mode energies in nuclei.

ACKNOWLEDGMENTS

One of us (M.V.S.) would like to thank the kind hospitality at TUM München. This work is partly supported by the EEC under Contract No. ERB-CHBI-CT93-0651 and the Bundesministerium für Forschung und Technologie in Bonn under the Project No. 06 TM733. We thank R. Behnsch for careful reading of the manuscript.

[1] M.M. Sharma, in *Nuclear Equation of State*, edited by W. Greiner and H. Stöcker (Plenum, New York, 1990), Vol. 216A, p. 661.

[2] H. Stöcker and W. Greiner, Phys. Rep. **137**, 277 (1986).

[3] M. Buenerd, in *Proceedings of the Nuclear Physics Workshop, ICTP, Trieste, Italy, 1981,* edited by C.H. Dasso, R.A. Broglia, and A. Winther (North-Holland, Amsterdam, 1982).

[4] M.M. Sharma, W.T.A. Borghols, S. Brandenburg, S. Crona, A. van der Woude, and M.N. Harakeh, Phys. Rev. C **38**, 2562 (1988).
[5] M.M. Sharma, W. Stocker, P. Gleissl, and M. Brack, Nucl. Phys. **A504**, 337 (1989).
[6] M.M. Sharma, "The Compressibility of Nuclear Matter Revisited: The Third Derivative of EOS from Breathing Mode," invited talk given at the Notre Dame Workshop on Giant Resonances and Related Phenomena, Notre Dame, Indiana, 1991 (Daresbury Laboratory Report No. DL/NUC/P323T, 1991) (unpublished).
[7] S. Shlomo and D.H. Youngblood, Phys. Rev. C **47**, 529 (1993).
[8] J.P. Blaizot, Phys. Rep. **64C**, 171 (1980).
[9] P. Gleissl, M. Brack, J. Meyer, and P. Quentin, Ann. Phys. (N.Y.) **197**, 205 (1990).
[10] J. Treiner, H. Krivine, O. Bohigas, and J. Martorell, Nucl. Phys. **A371**, 253 (1981).
[11] B.D. Serot and J.D.Walecka, Adv. Nucl. Phys. **16**, 1 (1986).
[12] Y.K. Gambhir, P. Ring, and A. Thimet, Ann. Phys. **198**, 132 (1990).
[13] M.M. Sharma, M.A. Nagarajan, and P. Ring, Phys. Lett. B **312**, 377 (1993).
[14] M.M. Sharma, G.A. Lalazissis, and P. Ring, Phys. Lett. B **317**, 9 (1993).
[15] M.M. Sharma, G.A. Lalazissis, W. Hillebrandt, and P. Ring, Phys. Rev. Lett. **72**, 1431 (1994).
[16] P. Möller, J.R. Nix, W.D. Myers, and W.J. Swiatecki, At. Data Nucl. Data Tables (in press).
[17] P. Haensel, J.L. Zdunik, and J. Dobaczewski, Astron. Astrophys. **222**, 353 (1989).
[18] J. Dobaczewski, I. Hamamoto, W. Nazarewicz, and J.A. Sheikh, Phys. Rev. Lett. **72**, 981 (1994).
[19] T. Maruyama and T. Suzuki, Phys. Lett. B **219**, 43 (1989).
[20] H.F. Boersma, R. Malfliet, and O. Scholten, Phys. Lett. B **269**, 1 (1991).
[21] M.V. Stoitsov, M. Cescato, P. Ring, and M.M. Sharma, submitted to J. Phys. G: Nucl. Phys.
[22] D.L. Hill and J.A. Wheeler, Phys. Rev. **89**, 1102 (1953).
[23] R.A. Ferrell and W.M. Visscher, Phys. Rev. **102**, 450 (1956).
[24] H. Flocard and D. Vautherin, Nucl. Phys. **A264**, 197 (1976).
[25] S. Krewald, R. Rosenfelder, J.E. Galonska, and A. Faessler, Nucl. Phys. **A269**, 112 (1976).
[26] J. Boguta and A.R. Bodmer, Nucl. Phys. **A292**, 413 (1977).
[27] H. Kucharek and P. Ring, Z. Phys. A **339**, 23 (1991).
[28] M.V. Stoitsov, M.M. Sharma, R. Behnsch, P. Ring, and S. Nishiyama, to be submitted to Ann. Phys. (N.Y.).
[29] P. Ring and P. Schuck, *The Nuclear Many-Body Problem* (Springer-Verlag, New York, 1980), Chap. 10.
[30] P. Bonche, J. Dobaczewski, H. Flocard, and P.-H. Heenen, Nucl. Phys. **A530**, 149 (1991).
[31] O. Bohigas, A.M. Lane, and J. Martorell, Phys. Rep. **51**, 276 (1979).
[32] P.G. Reinhard, Rep. Prog. Phys. **52**, 439 (1989).
[33] S.J. Lee, J. Fink, A.B. Balantekin, M.R. Strayer, A.S. Umar, P.-G. Reinhard, J.A. Maruhn, and W. Greiner, Phys. Rev. Lett. **57**, 2916 (1986).
[34] C.J. Horowitz and B.D. Serot, Nucl. Phys. **A368**, 503 (1981).
[35] M.M. Sharma, M.A. Nagarajan, and P. Ring, Ann. Phys. (N.Y.) **231**, 110 (1994).